2019

Highly Crystalline Zinc Oxide/Mesoporous Hollow Silica Composites Synthesized at Low Temperature for the Photocatalytic Degradation of Sodium Dodecylbenzenesulfonate

Parisa Pourdayhimi, *University Technology Malaysia*
Pei Wen Koh, *University Technology Malaysia*
Hadi Nur, *University Technology Malaysia*
Siew Ling Lee, *University Technology Malaysia*

CSIRO PUBLISHING

Aust. J. Chem. **2019**, *72*, 252–259
https://doi.org/10.1071/CH18175

Full Paper

Highly Crystalline Zinc Oxide/Mesoporous Hollow Silica Composites Synthesized at Low Temperature for the Photocatalytic Degradation of Sodium Dodecylbenzenesulfonate

Parisa Pourdayhimi,[A] *Pei Wen Koh,*[A] *Hadi Nur,*[B,C] *and Siew Ling Lee*[A,B,D]

[A]Department of Chemistry, Faculty of Science, Universiti Teknologi Malaysia, 81310 Johor Bahru, Johor, Malaysia.
[B]Center for Sustainable Nanomaterials, Ibnu Sina Institute for Scientific and Industrial Research, Universiti Teknologi Malaysia, 81310 Johor Bahru, Johor, Malaysia.
[C]Central Laboratory of Minerals and Advanced Materials, Faculty of Mathematics and Natural Science, State University of Malang, Malang 65145, Indonesia.
[D]Corresponding author. Email: sllee@ibnusina.utm.my

Highly crystalline ZnO/mesoporous hollow silica sphere (MHSS) composites have been successfully synthesized through an impregnation method at 323 K without applying calcination. Three composites of different Zn/Si molar ratios of 1 : 2, 1 : 1, and 2 : 1 were prepared. X-Ray diffraction patterns confirmed the presence of highly crystalline ZnO in the materials. A layer of ZnO was formed on the MHSS as evidenced by field emission scanning electron microscopy analysis. Transmission electron microscopy analysis verified the mesoporous structure in ZnO/MHSS composites. N_2 adsorption–desorption analysis indicated a type IV isotherm for 1ZnO/2MHSS and 1ZnO/1MHSS samples, confirming the presence of mesopores in the ZnO layer. It has been demonstrated that all the ZnO/MHSS composites exhibit a high photocatalytic activity towards sodium dodecylbenzenesulfonate degradation compared with bare ZnO under UV irradiation. A kinetic study showed that the photodegradation followed a second order model. Among the prepared composites, 1ZnO/1MHSS recorded the highest reaction rate of 6.03×10^{-3} mM^{-1} min^{-1} which is attributed to a high crystallinity and the monodispersity of a high amount of ZnO on MHSS.

Manuscript received: 18 April 2018.
Manuscript accepted: 4 December 2018.
Published online: 21 January 2019.

Introduction

Sodium dodecylbenzenesulfonate (SDBS) is commonly used as a surfactant in the manufacture of cleaning products. Its presence in water could cause the production of a large amount of foam, which hinders oxygen from dissolving into water and facilitates growth of harmful bacteria. Thus, SDBS should be removed before disposal. In fact, the photodegradation of SDBS in aqueous suspensions of TiO_2 powder, Degussa P-25, and TiO_2–SiO_2 have been reported.[1–3] Unfortunately, the photocatalytic activity of these TiO_2-based materials was limited due to their low surface area and porosity.

In the last two decades, the photocatalytic degradation of organic contaminants is considered as a promising approach for environmental clean-up applications.[4–6] Semiconductor photocatalysis has attracted a lot of attention since it involves milder operating conditions of temperature and pressure, low cost, and the possibility of using solar energy to drive the process. Similar to TiO_2, ZnO with a wide direct bandgap (3.37 eV) is among the most efficient photocatalysts. ZnO is a kind of environmentally friendly, cheap, and biocompatible material and it is listed as a safe material by the US Food and Drug Administration (21CFR182.8991).[7] However, ZnO nanoparticles tend to aggregate and form an irregular shape morphology which destabilises the catalyst and retards the activity.[8] An established solution to address the aggregation problem is to distribute the nanoparticles into/onto a porous, chemically inert, and preferably high surface area support.

Mesoporous materials have commonly been used as supports for different metal oxide nanoparticles for improved catalytic performances over their non-supported analogues.[9,10] Various silica supports have been intensively applied in heterogeneous catalyst design by many researchers due to their easy preparation, good compatibility with other materials, and good environmental stability.[11–15] A literature study showed an increasing trend in synthesizing ZnO nanoparticles loaded onto or into mesoporous supports. For instance, mesoporous silica impregnated with an ethanolic/aqueous solution of zinc nitrate was reported.[16] Thermal treatment up to 973 K allowed the evolution of samples and dispersion of ZnO nanocrystalline particles onto the mesoporous silica. On the other hand, ZnO was immobilized in mesoporous SBA-15 where a high loading of ZnO clusters was distributed in the channels of SBA-15.[17]

Recently, ZnO was successfully dispersed homogeneously onto mesoporous silica KIT-6 and attained a high catalytic reaction in quinoxalines production.[18]

It was documented that a high crystallinity favoured the photoactivity of ZnO.[19] Usually, a post heat treatment at elevated temperatures was needed to obtain crystallized ZnO. In most of the cases, the heat treatment tended to cause agglomeration of nanoparticles, resulting in an increase of the nanoparticles' size and decrease in surface area.[20–22] Therefore, a simple preparation method to produce well crystallized ZnO supported on a mesoporous silica material without applying heat treatment is strongly favoured.

Mesoporous hollow silica spheres (MHSSs) are receiving much attention owing to their low density, low toxicity, and large surface area. MHSSs have been employed as a support for nanoparticle immobilization.[21–25] In our previous work,[25] a low amount of ZnO (~2–6 mol-%) was immobilized on MHSS via a wet impregnation method followed by a post heat treatment at 973 K for 3 h. The good distribution of ZnO nanoparticles on a MHSS support enhanced the photodegradation efficiency of SDBS. However, high temperature calcination limited more ZnO loading due to formation of zinc silicate which was unfavourable. In addition, the very low crystallinity of the materials has restricted their photocatalytic activity. In the current study, therefore, highly crystalline ZnO/MHSS composites of a high ZnO content were synthesized via a simple preparation method at low temperature. The properties and photocatalytic activity of these composites are presented.

Experimental

Synthesis of ZnO Nanoparticles and MHSS

ZnO nanoparticles were prepared through a sol–gel method as described elsewhere.[25,26] In a typical reaction, 0.1 M zinc acetate dihydrate solution was added to a 0.15 M hydrazine hydrate ($N_2H_4{\cdot}H_2O$) solution, followed by stirring for 15 min at room temperature. The reaction mixture was kept at 323 K for 3 h. The obtained white colloidal solution was centrifuged, filtered off, and washed with deionized water and ethanol before drying in an oven at 353 K.

To prepare the MHSSs through a sol–gel emulsion method, typically, a 43 mL mixture of water and ethanol, 0.5 mL of TEOS, and 0.1175 g of cetyl trimethylammonium bromide (CTAB) were mixed followed by the addition of 0.5 mL of ammonia solution (25 wt-% NH_3 in water) under a medium speed of stirring for 24 h. The white precipitate was collected centrifugally, washed with a mixture of water and ethanol, and calcined in air at 873 K for 6 h.

Synthesis of ZnO/MHSS Composites

In order to synthesize ZnO/MHSS composites, zinc acetate dihydrate ($Zn(CH_3COO)_2{\cdot}2H_2O$) (GCE Laboratory Chemicals, 99 %) and hydrazine hydrate ($N_2H_4{\cdot}H_2O$) (Sigma Aldrich, 50–60 %) solutions were used. Three molar ratios of Zn/Si precursors (1 : 2, 1 : 1, and 2 : 1) were employed to investigate the effect of loading percentage of ZnO on the catalyst properties and performance. In a typical reaction, MHSS powder (0.5 g) was dispersed in a proper amount of distilled water under stirring overnight, followed by addition of zinc acetate dihydrate powder. The mixture was then stirred for another 10 min and heated to 323 K before addition of 0.15 M hydrazine hydrate solution. The reaction mixture was heated at 323 K for 2 h. Finally, the white precipitate was filtered off, washed with distilled water, and dried at 353 K in an oven overnight. The resulting samples were labelled as xZnO/yMHSS, where x and y represent the molar ratio of Zn and MHSS, respectively, in the samples.

Characterization

Phase determination was conducted on a Bruker Advance D8 X-ray diffractometer equipped with Cu Kα radiation (λ 0.15406 nm, 40 kV, 40 mA). The crystallite size of the samples was calculated based on Scherrer's equation. Transmission electron microscopy (TEM) (JEM-2100, 200 kV) was used to examine the hollowness and mesoporous characteristics of the MHSS and ZnO/MHSS samples. The morphology and particle size of the prepared samples were obtained by field emission scanning electron microscopy (FESEM) (Carls Ziess 35VP). Textural properties of the prepared samples were characterized with a Quantachrome Surface Autosorb-6B sorption analyzer at 77 K. Inductively coupled plasma optical emission spectroscopy (ICP-OES) (Agilent Technologies, 700 Series) was used to determine the zinc content in the composites. FT-IR spectra were recorded with a scan range of 400–4000 cm^{-1} on a Nicolet iS10 spectrometer equipped with an attenuated total reflectance accessory. Optical properties of the samples were investigated with a Perkin Elmer Ultraviolet-visible spectrometer Lambda 35 series in the wavelength range of 200–900 nm using barium sulfate ($BaSO_4$) as a reference.

Photocatalytic Testing

The photocatalytic performance of the synthesized ZnO/MHSS composites was tested by the photodegradation of SDBS. The prepared photocatalysts (0.1 g) were added to 500 mL of 30 ppm SDBS (Sigma Aldrich, 95 % mixture of isomers). Prior to the photocatalytic testing, an adsorption test was carried out at neutral pH in the dark for 2 h to achieve equilibrium. The suspension was irradiated using a UVc lamp (16 W, 254 nm wavelength). In order to trace the photodegradation reaction, sampling was carried out at determined time intervals by using a syringe. A millipore membrane filter (0.2 μm) was used to filter the sample particles. The concentration of the filtrate was determined using a Shimadzu UV-1601PC UV-vis spectrophotometer, measured at the maximum wavelength of SDBS at 224 nm. The efficiency of the photocatalytic activity was calculated using the equation $(C_0 - C_t)/C_0 \times 100\,\%$, where C_0 and C_t are the concentration of the SDBS solution before the reaction and at the relevant time interval, respectively. For comparison purposes, the photocatalytic behaviour of ZnO and MHSS was also evaluated. Finally, the reusability of the best photocatalyst was evaluated. In the reusability test, the photocatalyst was reused for the photodegradation of fresh SDBS solution for each cycle. The reaction conditions including the initial concentration of SDBS (500 mL 30 ppm) and reaction time (2 h irradiation) were kept constant for all the cycles. In order to recover the photocatalyst, it was centrifuged, washed, and dried at 373 K for every cycle.

Results and Discussion

Phase Determination

Fig. 1 depicts XRD patterns of the synthesized ZnO, ZnO/MHSS composites, and MHSS. For ZnO (Fig. 1a), a series of peaks were detected at 31.9° (100), 34.5° (002), 36.5° (101), 47.6° (102), 56.7° (110), 63.0° (103), 66.5° (200), 68.1° (112), and 69.1° (201), which could be indexed as a wurtzite ZnO

structure (JCPDS No. 36-1451).[27] The effect of ZnO loaded into/onto MHSS was investigated. The peak at 2θ 3.19° (Fig. 1a) which is associated with the mesoporous silica structure,[25] disappeared in the ZnO/MHSS composite materials (Fig. 1b–d). This could be due to the coverage of loaded ZnO on the surface of MHSS.

The presence of a broad peak at 2θ 7.1° and a hump at 2θ 22.0° correspond to the amorphous silica (Fig. 1e) which were also reported previously.[28] Upon introduction of zinc oxide, these two peaks shifted to a lower degree at 2θ 6.5° and 13.5° respectively. The shift was indicative of a significant change in silica structure due to the introduction of zinc oxide to the silica framework.[28]

All the ZnO/MHSS composites showed obvious sharp diffraction peaks that corresponded to a well crystallized wurtzite ZnO structure, suggesting the structure of ZnO was well maintained even after loading onto the MHSS support. In 2ZnO/1MHSS (Fig. 1b), the formation of ZnO along the (002) diffraction plane was dominant, implying the preferred orientation. Meanwhile, in the case of 1ZnO/1MHSS and 1ZnO/2MHSS ((Fig. 1c, d), the growth of ZnO along the (101) diffraction plane was preferred. The sharper diffraction peaks of 1ZnO/1MHSS corresponded to the higher crystallinity in the sample.

The crystallite size of ZnO and all the ZnO/MHSS samples was determined from the peak of maximum intensity using the Scherrer formula. Since MHSS is amorphous silica, it has no crystalline phase. Meanwhile, the ZnO nanoparticles have a crystallite size of 22.7 nm. After the introduction of ZnO onto MHSS, the crystallite size decreased to 18.7 and 17.9 nm for 1ZnO/2MHSS and 1ZnO/1MHSS, respectively. Conversely, a larger crystallite size of 24.3 nm was recorded for 2ZnO/1MHSS.

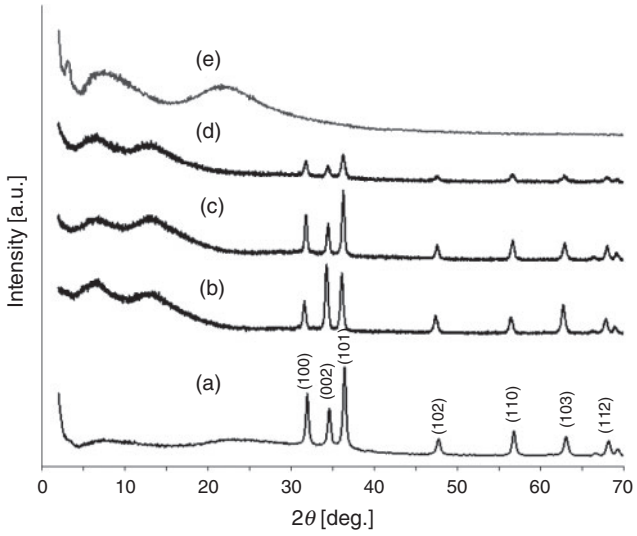

Fig. 1. XRD patterns of (a) ZnO, (b) 2ZnO/1MHSS, (c) 1ZnO/1MHSS, (d) 1ZnO/2MHSS, and (e) MHSS.

Morphological Studies

Fig. 2 shows TEM images of the 1ZnO/1MHSS composite. The images clearly demonstrate the mesoporous structure of the spherical 1ZnO/1MHSS composite with an approximate diameter of 250 nm. The mesoporous structure in the TEM image of 1ZnO/1MHSS might be related to the presence of mesopores in the ZnO layer. Based on XRD analysis, the peak related to the mesoporous structure of silica (2θ 3.19°) has disappeared, implying that the MHSS mesopores have been filled with ZnO.

In our previous report,[25] uniform and monodisperse porous MHSS with an average diameter of 108 nm was obtained with the current applied synthesis method. The hollowness and porosity properties of MHSS and all Zn/MHSS composites were confirmed as evidenced by the TEM analysis. Similar images of MHSS were reported previously.[29,30]

FESEM images of the ZnO/MHSS materials are shown in Fig. 3. The average particle size of each sample was determined by considering 20 particles of each sample in the FESEM images. According to the images (Fig. 3a–c), the average particle size increased in all the composites where 1ZnO/2MHSS, 1ZnO/1MHSS, and 2ZnO/1MHSS possessed average values of 143, 339, and 571 nm, respectively. By comparing the average particle sizes of ZnO (55 nm) and MHSS (105 nm) as reported previously,[25] the significant increase in particle sizes of the ZnO/MHSS composites might imply the existence of the ZnO layer on the surface of MHSS. In contrast, it was documented that ZnO was dispersed in the pores of MHSS when the ZnO loading was carried out through the impregnation method followed by calcination at a high temperature of 973 K for 3 h.[25]

For the 1ZnO/2MHSS and 1ZnO/1MHSS composites (Fig. 3a, b), the uniform and monodispersed spherical particles of MHSS have been thoroughly covered with fine ZnO nanoparticles with the least particle aggregation. However, in the case of 2ZnO/1MHSS (Fig. 3c), a remarkable amount of aggregates is clearly observed, implying that the amount of ZnO precursor applied was in excess and as such the ZnO located inside and outside of the MHSS and also beyond the surface capacity of MHSS, leading to a non-uniform morphology. Some aggregates were also observed in the 1ZnO/2MHSS

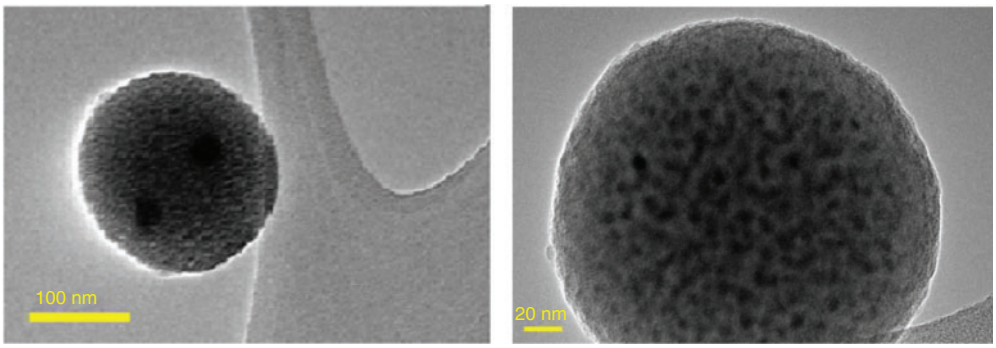

Fig. 2. TEM images of the 1ZnO/1MHSS composite.

sample. The current findings strongly denote that an optimized molar ratio of ZnO to MHSS is important for a highly uniform monodispersion of ZnO immobilized on MHSS without particle aggregation.

Study of Textural Properties and Determination of Zn Content

The textural properties of MHSS and ZnO/MHSS samples were examined via N_2 adsorption–desorption analysis. The specific surface areas, average pore volume, and pore size of ZnO, MHSS, and the ZnO/MHSS composites are listed in Table 1. The MHSS possessed a large surface area of 1029 $m^2\ g^{-1}$. A significant decrease in surface area was observed after loading of ZnO onto MHSS where the surface area of the composites ranged from 44 to 82 $m^2\ g^{-1}$. Similarly, the pore volume of MHSS decreased dramatically with the presence of ZnO. The results might imply blockage of pores due to the formation of a ZnO layer on the surface of MHSS.

The isotherms of the samples are depicted in Fig. 4. As can be seen in Fig. 4a, MHSS demonstrated a type IV isotherm.[31] A distinct step was observed at a relative pressure of 0.3 with a total absence of hysteresis. In a previous report, MCM-41 was claimed to possess a similar isotherm with pores of 2.5 nm.[32] Zhu et al.[33] reported a type IV isotherm curve with a well defined step between 0.2 and 0.3 of P/P_0 for MHSSs. Similar type IV isotherms were also obtained for MHSSs by other researchers.[29,34]

After the introduction of ZnO, 1ZnO/2MHSS and 1ZnO/1MHSS maintained their type IV isotherm (Fig. 4b).[31] The amount of adsorbed gas in the 1ZnO/1MHSS has the highest value among the three ZnO/MHSS composites. This can be explained by the higher surface area and total pore volume of 1ZnO/1MHSS as compared with 1ZnO/2MHSS and 2ZnO/1MHSS. 2ZnO/1MHSS showed a type II isotherm according to the IUPAC classification, indicating a non-porous material due to the presence of aggregation. This finding was in agreement with the FESEM image (Fig. 3f).

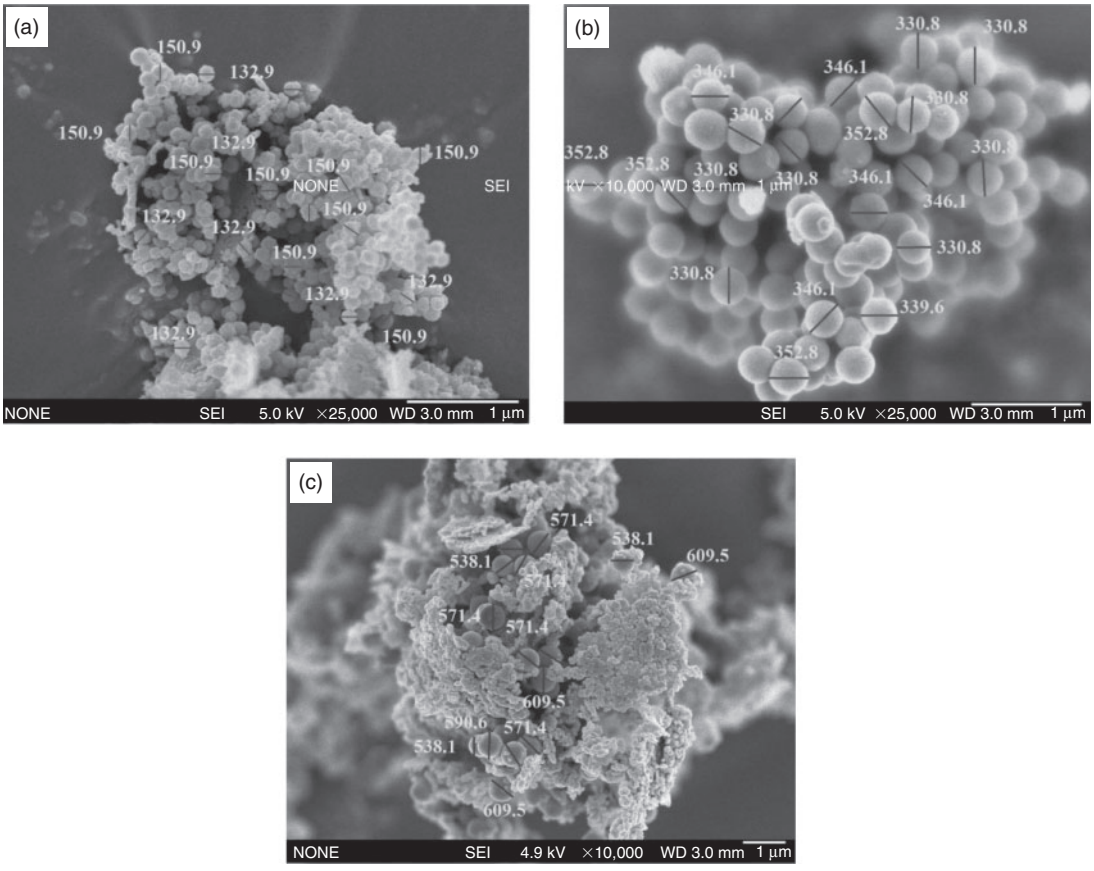

Fig. 3. FESEM images of (a) 1ZnO/2MHSS, (b) 1ZnO/1MHSS, and (c) 2ZnO/1MHSS.

Table 1. Textural properties and Zn content of the materials

Sample	Surface area [$m^2\ g^{-1}$]	Pore size diameter [nm]	Pore volume [$cm^3\ g^{-1}$]	Zn content[A] [wt-%]	Zn $content_{Theor}$ [wt-%]
ZnO	39	—	—	—	—
1ZnO/2MHSS	44	19.95	0.10	19.5	40.4
1ZnO/1MHSS	82	11.79	0.22	25.0	57.5
2ZnO/1MHSS	54	9.01	0.09	34.3	73.0
MHSS	1029	2.61	0.77	—	—

[A]Determined through ICP-OES analysis. The analysis was only carried out on ZnO/MHSS composites.

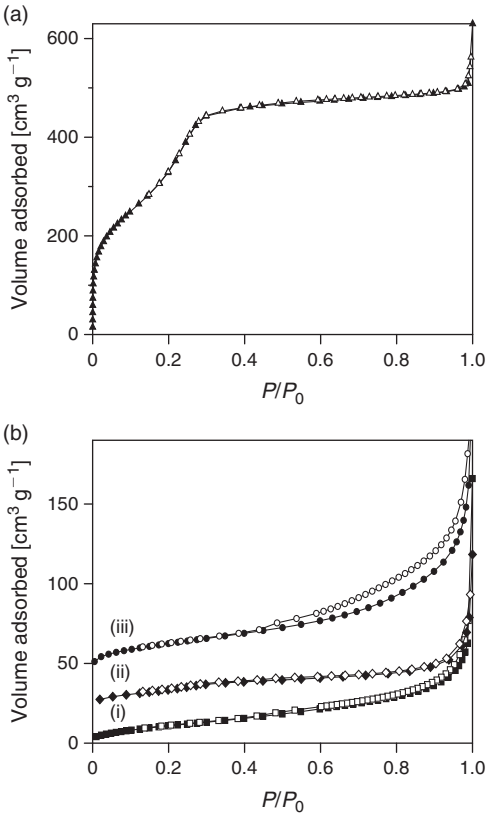

Fig. 4. Isotherm plots of (a) MHSS and (b) ZnO/MHSS composites: (i) 1ZnO/2MHSS, (ii) 2ZnO/1MHSS, and (iii) 1ZnO/1MHSS. (Filled points are adsorption isotherms, empty points are desorption isotherms. Curves (ii) and (iii) are marginally moved upwards by 40 and 20 $cm^3\ g^{-1}$, respectively, for clearer presentation.)

The isotherm plot of 1ZnO/1MHSS shows a very wide hysteresis loop, type H3 at relative pressures of 0.44–1.0, which corresponded to the capillary condensation of nitrogen gas in the mesopores with an average pore size of 11.79 nm and pore volume 0.22 $cm^3\ g^{-1}$. The wide H3 hysteresis loop could be related to a more random distribution of pores and interconnected pore systems.[32,35] Subsequently, this interconnected pore system led to the increased total pore volume and surface area in sample 1ZnO/1MHSS.

In the case of 2ZnO/1MHSS, the Brunauer–Emmett–Teller (BET) surface area, pore size, and Barrett-Joyner-Halenda (BJH) pore volume obtained were 54 $m^2\ g^{-1}$, 9.01 nm, and 0.09 $cm^3\ g^{-1}$, respectively. Meanwhile, the absence of a hysteresis loop in sample 2ZnO/1MHSS may imply that active ZnO has filled the pores of MHSS. This was in good agreement with the decrease of pore volume from 0.22 to 0.09 $cm^3\ g^{-1}$ after the Zn content increased from 25 to 34.3 wt-%. The BET surface area, pore size, and BJH pore volume of 1ZnO/2MHSS were 44 $m^2\ g^{-1}$, 19.95 nm, and 0.10 $cm^3\ g^{-1}$, respectively.

The content of Zn in the prepared composites was examined by ICP-OES analysis and the results are shown in Table 1. As observed, the obtained values of weight percentages of Zn were 19.5, 25.0, and 34.3 wt-% for 1ZnO/2MHSS, 1ZnO/1MHSS, and 2ZnO/1MHSS, respectively. By comparing the obtained mass percentage to the corresponding theoretical values, it was obvious that the experimental values were smaller than the expected values. This was probably due to less availability of active sites such as silanol (Si–OH) and siloxane (Si–O–Si) on

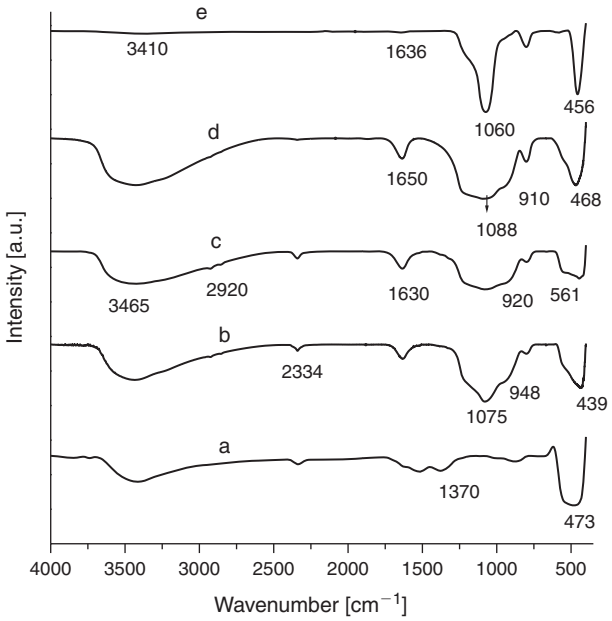

Fig. 5. Infrared spectra of (a) ZnO, (b) 2ZnO/1MHSS, (c) 1ZnO/1MHSS, (d) 1ZnO/2MHSS, and (e) MHSS.

the surface of MHSS to interact with hydrazine hydrate and ZnO precursors through hydrogen bonding.[25] Consequently, it might have caused the loss of ZnO during the impregnation process.

Vibrational Spectroscopy

Fig. 5 shows the FTIR spectra of ZnO, MHSS, and the ZnO/MHSS samples. In Fig. 5a, the peak at 442 cm^{-1} was assigned to the stretching frequency of a Zn–O bond. The absorption bands at 2920 and 2334 cm^{-1} were attributed to C–H and C–O, while peaks observed at 1570, 1412, and 1336 cm^{-1} were assigned to the asymmetrical and symmetrical stretching of the zinc carboxylate, respectively. The results indicated the presence of unreacted zinc acetate in the sample. Similar observations have been claimed for ZnO in previous reports.[36,37]

The bands at around 3410 and 1636 cm^{-1} were attributed to the stretching and bending modes of the O–H band of the silanol group. Apparently, these bands are not noticeable in MHSS (Fig. 5e). The absence of O–H groups in MHSS might explain the insufficient active sites for attachment of ZnO on the surface of MHSS, resulting in low a wt-% of ZnO in the prepared composites (Table 1). For MHSS, three obvious characteristic vibrations of siloxane bands were observed. The band at 1060 cm^{-1} corresponded to the asymmetric stretching mode of Si–O–Si, while the absorption bands at 806 and 456 cm^{-1} were attributed to symmetric stretching and bending vibrational modes of Si–O–Si, respectively.[34,38] After introduction of ZnO to MHSS, the intensity of the absorption bands at around 3410 and 1636 cm^{-1} increased, implying the presence of more hydroxy groups and absorbed water. In all the ZnO/MHSS samples, the absorption peaks shifted to higher frequency, implying the possible interaction between the O–H band of the silanol group or surface adsorbed water with ZnO. All the ZnO/MHSS composites exhibited very broad peaks for the asymmetric stretching vibration of the Si–O–Si band. The broadening of these peaks could be due to the existence of strong hydrogenic bands between the O–H band of the silanol

Table 2. Values of wavelength and bandgap energy of ZnO and ZnO/MHSS composites

Sample	Wavelength [nm]	Bandgap energy [eV]
ZnO	387	3.20
1ZnO/2MHSS	385	3.22
1ZnO/1MHSS	385	3.22
2ZnO/1MHSS	392	3.16

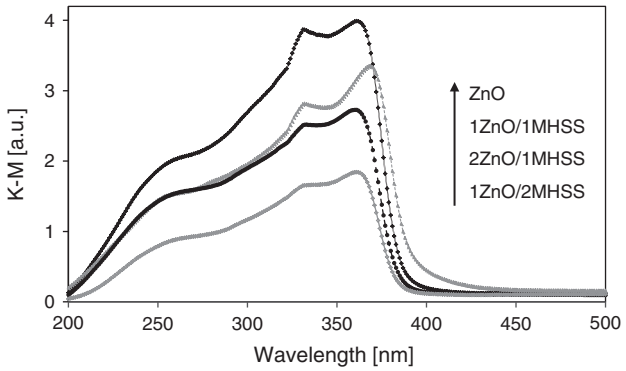

Fig. 6. DR UV-Vis spectra of ZnO and the ZnO/MHSS composites.

group or surface adsorbed water with the Si–O–Si band in the framework of silica which in turn caused higher vibrations of the oxygen atom of the siloxane group.[35]

In addition, a band at 920–948 cm^{-1} that corresponded to Si–O–H bending appeared upon introduction of ZnO in all the ZnO/MHSS samples. The increased intensity in this region with increasing ZnO content is a good indication of more Si–O–Zn interactions.[32,39]

Diffuse Reflectance UV-Visible Spectroscopy

Fig. 6 depicts the diffuse reflectance UV-visible (DR UV-vis) spectra of ZnO, 2ZnO/1MHSS, 1ZnO/1MHSS, and 1ZnO/2MHSS. ZnO nanoparticles showed a strong absorption in the UV region with a maximum at 364 nm which is associated with the electronic transition from the valence band of oxygen to the conduction band of the zinc atom. It is also related to the intrinsic bandgap of ZnO.[40] The bandgap energies of the prepared samples are tabulated in Table 2. The wavelength and bandgap energy of ZnO obtained were 387 nm and 3.20 eV, respectively. It is observable from Fig. 6 that 1ZnO/2MHSS and 1ZnO/1MHSS have a similar bandgap energy to that of bare ZnO. This finding is probably due to the formation of fine ZnO particles on the MHSS surface which is in agreement with FESEM images (Fig. 3). Meanwhile, it was believed that the larger particle size of 2ZnO/1MHSS (with an average diameter of 571 nm) compared to 1ZnO/2MHSS (143 nm) and 1ZnO/1MHSS (339 nm) samples might have contributed to the slight red-shift in the DR UV-vis spectrum and lower bandgap energy (3.16 eV) for 2ZnO/1MHSS. In fact, these ZnO/MHSS composites have a very similar bandgap energy. A similar effect of grain size on the bandgap energy of semiconductors has been reported.[41]

Photodegradation of SDBS

An adsorption test demonstrated that all the photocatalysts reached equilibrium after 2 h in the dark. MHSS and all the prepared ZnO/MHSS composites adsorbed ~0.008 mM SDBS (or 10 %). The photocatalytic testing was carried out through photodegradation of the remaining SDBS in the reactor using the ZnO/MHSS composites, ZnO, and MHSS as photocatalysts. As illustrated in Fig. 7, all the photocatalysts exhibited a sharp increase of SDBS photodegradation percentage in the first hour of reaction, suggesting a high reaction rate. A slower reaction rate was observed after 1.5 h of reaction. Apparently, 1ZnO/1MHSS was the best photocatalyst for SDBS photodegradation, followed by 2ZnO/1MHSS, 1ZnO/2MHSS, and ZnO.

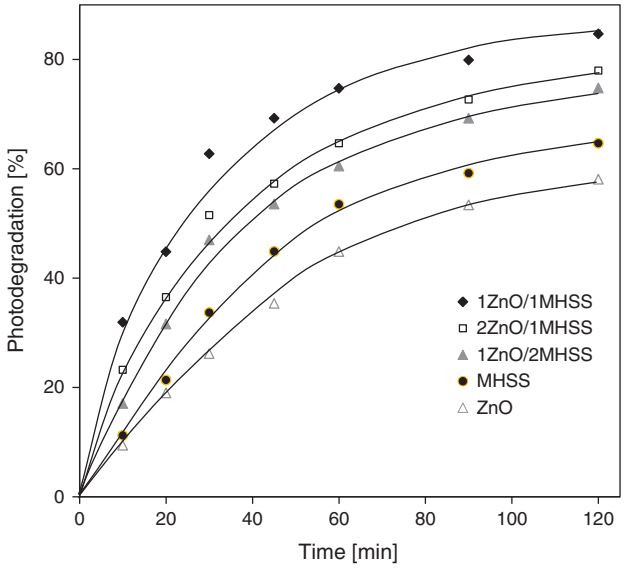

Fig. 7. Photocatalytic degradation of SDBS using MHSS, ZnO, and the ZnO/MHSS samples.

The lowest photocatalytic efficiency of ZnO was attributed to aggregation of particles as evidenced by the FESEM image of ZnO. In this work, the loading of ZnO nanoparticles onto MHSS has prevented ZnO from aggregation, leading to formation of composite particles of uniform spherical shape and narrow size distribution. The current results demonstrated that the photocatalytic activity of ZnO significantly increased by 16.7–26.7 % through distribution of ZnO nanoparticles over the high surface area MHSS.

On the other hand, the high catalytic activity of ZnO/MHSS composites could be explained by the isoelectric point (IEP) of ZnO and existence of many hydroxy groups (as evidenced by FTIR results). ZnO possesses an isoelectric point ranging from 8.7 to 10.3.[42,43] This means that at neutral pH, which is lower than the IEP of ZnO, protons from the environment could be easily transferred to the particle surface, forming $ZnOH_2^+$ groups with a positive charge on the surface of the ZnO layer.[44,45] Therefore, the SDBS anions present in solution would be attracted by the positive surface of ZnO, hence increasing SDBS adsorption during the dark adsorption and photocatalysis process. Meanwhile, the hydroxy groups could have contributed to production of more $^{\bullet}OH$ radicals, thus accelerating the photocatalytic reaction for all ZnO/MHSS samples. In the case of 1ZnO/1MHSS, the higher crystallinity, uniformity, and monodispersity of spherical particles as well as higher surface area and pore volume of this sample would have provided an optimum condition for the photocatalytic reaction.

The kinetic study of the photodegradation of SDBS was conducted using the bare ZnO and ZnO/MHSS photocatalysts.

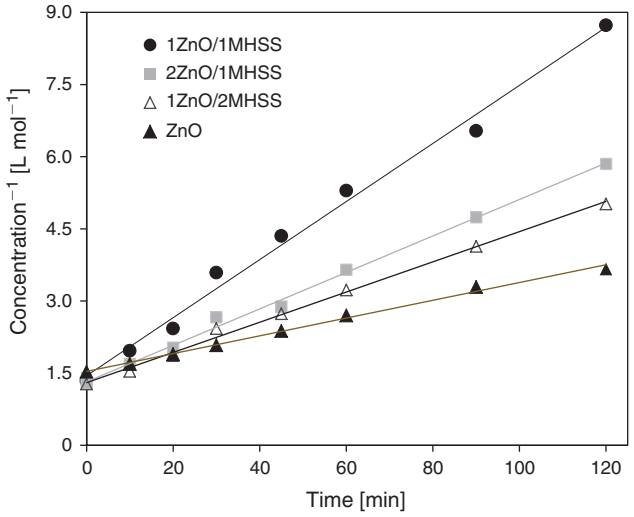

Fig. 8. Photodegradation kinetics of SDBS using different ZnO/MHSS photocatalysts.

As shown in Fig. 8, the plot of $1/C_t$ versus irradiation time gave good linearity with high R^2 (> 0.99), verifying that the reaction process followed a second order kinetics model, which is commonly expressed by Eqn 1:

$$1/C_t = kt + 1/C_0 \quad (1)$$

where k is the second order rate constant and C_0 and C_t are the concentrations of SDBS at the initial time and time t, respectively.[46]

The data were fitted to the corresponding linear expression to obtain an apparent rate constant, k. Values of k when using ZnO and ZnO/MHSS photocatalysts are tabulated in Table 3. For comparison purposes, normalized k values (k') with respect to the surface area of the catalyst were calculated, which corresponded to the values of rate constants without considering the surface area effect on the photocatalyst performance. The higher value of k' of 1ZnO/1MHSS (7.44×10^{-5} mM^{-1} min^{-1}) strongly suggested that an optimized ratio of Zn/Si is crucial for the better photocatalytic activity of the ZnO/MHSS composite in the photodegradation of SDBS.

It is worth noting that although 1ZnO/1MHSS has a lower surface area than that of ZnO/15MHSS (90 m^2 g^{-1}),[25] it has a higher photocatalytic activity. 1ZnO/MHSS photodegradated 74.7% of SDBS while ZnO/15MHSS photodegraded only 68.6% of SDBS after 1 h reaction under UV light irradiation. In addition, 1ZnO/1MHSS showed a higher reaction rate (6.03×10^{-3} mM^{-1} min^{-1}) as compared with that of ZnO/15MHSS (4.08×10^{-3} mM^{-1} min^{-1}) under the same reaction conditions. The current research findings strongly indicate that the enhanced activity is due to the high ZnO amount and high crystallinity of the ZnO/MHSS composites which were achieved through the low temperature synthesis.

Reusability of the Catalyst

The reusability of the best photocatalyst (1ZnO/1MHSS) was examined through employing recycling experiments. As shown in Fig. 9, 1ZnO/1MHSS was effective in the photodegradation of SDBS with a negligible photodegradation percentage drop (<5.9%) even after five cycles. The slight decrease in photocatalytic activity was probably due to catalyst aggregation after several cycles.

Table 3. The kinetic parameters of photodegradation of SDBS using ZnO and ZnO/MHSS photocatalysts

Catalyst	R^2	$k \times 10^{-3}$ [mM^{-1} min^{-1}]	$k' \times 10^{-5}$ [mM^{-1} min^{-1}]
ZnO	0.9949	1.85	4.74
1ZnO/2MHSS	0.9960	3.14	7.16
1ZnO/1MHSS	0.9912	6.03	7.44
2ZnO/1MHSS	0.9958	3.79	6.99

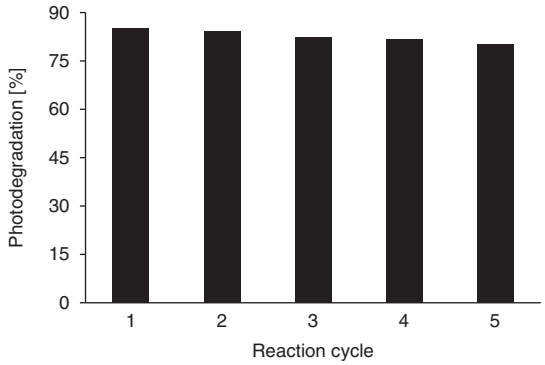

Fig. 9. Reusability of 1ZnO/1MHSS for the photodegradation of SDBS.

Conclusion

Highly crystalline ZnO/MHSS composites were successfully synthesized for the first time via an impregnation method at 323 K without applying calcination. In contrast to previously reported ZnO/MHSS composites which were prepared at a high temperature of 973 K,[25] this low temperature synthesis appeared to be a promising approach to produce ZnO of high crystallinity as well as hollow MHSSs with a high porosity as observed in the resulting composites. In addition, the low temperature synthesis allowed a higher loading of ZnO onto MHSS. It has been demonstrated that the crystalline ZnO/MHSS composites were good photocatalysts for photodegrading SDBS under UV light irradiation. The SDBS photodegradation efficiency of ZnO was enhanced by 16.7–26.7% with the presence of a MHSS support. The molar ratio a Zn to Si appeared to be a key factor in affecting the properties of the ZnO/MHSS composites. Among the prepared materials, 1ZnO/1MHSS was the best photocatalyst which photodegraded 74.7% of SDBS after 1 h of reaction. A kinetic study demonstrated that the photocatalytic reaction followed the second order model.

Conflicts of Interest

The authors declare no conflicts of interest.

Acknowledgements

The authors thank the Ministry of Higher Education (MOHE) and Universiti Teknologi Malaysia (UTM) for the financial support through research university grants (cost centre codes Q.J130000.2526.12H77, Q.J130000.2526.13H52, Q.J130000.2526.16H17 and Q.J130000.21A2.03E61). P. Pourdayhimi acknowledges the guidance from the late Professor Dr Alias Mohd Yusof (UTM). P.W. Koh is grateful for the post-doctoral fellowship sponsored by UTM.

References

[1] H. Hidaka, S. Yamada, S. Suenaga, H. Kubota, N. Serpone, E. Pelizzetti, M. Gratzel, *J. Photochem. Photobiol. Chem.* **1989**, *47*, 103. doi:10.1016/1010-6030(89)85010-5

[2] N. N. Rao, S. Dube, *J. Mol. Catal. Chem.* **1996**, *104*, L197. doi:10.1016/1381-1169(95)00259-6

[3] Y. Maryami, R. K. Tjoktronegoro, W. Suratno, S. Rochani, Third International Conference on Mathematics and Natural Sciences (ICMNS 2010) **2010**, Indonesia.

[4] M. R. Hoffmann, S. T. Martin, W. Choi, D. W. Bahnemann, *Chem. Rev.* **1995**, *95*, 69. doi:10.1021/CR00033A004

[5] P. W. Koh, M. H. M. Hatta, S. T. Ong, L. Yuliati, S. L. Lee, *J. Photochem. Photobiol. Chem.* **2017**, *332*, 215. doi:10.1016/J.JPHOTOCHEM.2016.08.027

[6] S. Mostoni, V. Pifferi, L. Falciola, D. Meroni, E. Pargoletti, E. Davoli, G. Cappelletti, *J. Photochem. Photobiol. Chem.* **2017**, *332*, 534. doi:10.1016/J.JPHOTOCHEM.2016.10.003

[7] T. Jin, D. Sun, H. Zhang, H.-J. Sue, in *Nanotoxicity* (Eds S. C. Sahu, D. A. Casciano) **2009**, pp. 81–95 (John Wiley & Sons, Ltd: Chichester).

[8] M. Elimelech, J. Gregory, X. Jia, R. A. Williams, *Particle Deposition and Aggregation: Measurement, Modelling and Simulation* **2013** (Butterworth-Heinemann: Oxford).

[9] L. Jiang, L. Gao, *Mater. Chem. Phys.* **2005**, *91*, 313.

[10] D. Kibanova, M. Trejo, H. Destaillats, J. Cervini-Silva, *Appl. Clay Sci.* **2009**, *42*, 563. doi:10.1016/J.CLAY.2008.03.009

[11] J. Taghavimoghaddam, G. P. Knowles, A. L. Chaffee, *J. Mol. Catal. Chem.* **2012**, *358*, 79. doi:10.1016/J.MOLCATA.2012.02.014

[12] J. Aguado, R. v. Grieken, M.-J. López-Muñoz, J. Marugán, *Appl. Catal. A* **2006**, *312*, 202. doi:10.1016/J.APCATA.2006.07.003

[13] Y. K. Ooi, L. Yuliati, S. L. Lee, *Chin. J. Chem.* **2016**, *37*, 1871.

[14] Y. K. Ooi, L. Yuliati, D. Hartanto, H. Nur, S. L. Lee, *Microporous Mesoporous Mater.* **2016**, *225*, 411. doi:10.1016/J.MICROMESO.2016.01.016

[15] S. C. Me, H. Nur, S. L. Lee, *Malaysian Journal of Fundamental and Applied Sciences* **2015**, *11*, 122.

[16] C. Cannas, M. Mainas, A. Musinu, G. Piccaluga, *Compos. Sci. Technol.* **2003**, *63*, 1187. doi:10.1016/S0266-3538(03)00040-X

[17] Q. Lu, Z. Wang, J. Li, P. Wang, X. Ye, *Nanoscale Res. Lett.* **2009**, *4*, 646. doi:10.1007/S11671-009-9294-X

[18] O. Hamid, M. A. Chari, C. V. Nguyen, J. E. Chen, S. M. Alshehri, E. Yanmaz, M. S. A. Hossain, Y. Yamauchi, K. C.-W. Wu, *Catal. Commun.* **2017**, *90*, 111. doi:10.1016/J.CATCOM.2016.10.026

[19] T. R. Giraldi, G. V. Santos, V. R. Mendonça, C. Ribeiro, I. T. Weber, *J. Nanosci. Nanotechnol.* **2011**, *11*, 3635. doi:10.1166/JNN.2011.3801

[20] M. Thirumavalavan, K.-L. Huang, J.-F. Lee, *Materials* **2013**, *6*, 4198. doi:10.3390/MA6094198

[21] A. Moballegh, H. R. Shahverdi, R. Aghababazadeh, A. R. Mirhabibi, *Surf. Sci.* **2007**, *601*, 2850. doi:10.1016/J.SUSC.2006.12.012

[22] J. Ye, R. Zhou, C. Zheng, Q. Sun, Y. Lv, C. Li, X. Hou, *Microchem. J.* **2012**, *100*, 61. doi:10.1016/J.MICROC.2011.09.002

[23] O. Verho, H. Zheng, K. P. J. Gustafson, A. Nagendiran, X. Zou, J.-E. Bäckvall, *ChemCatChem* **2016**, *8*, 773. doi:10.1002/CCTC.201501112

[24] J. Wang, C. Liu, L. Tong, J. Li, R. Luo, J. Qi, Y. Li, L. Wang, *RSC Adv.* **2015**, *5*, 69593. doi:10.1039/C5RA10826H

[25] P. Pourdayhimi, P. W. Koh, M. M. Salleh, H. Nur, S. L. Lee, *Aust. J. Chem.* **2016**, *69*, 790. doi:10.1071/CH15495

[26] K. Han, Z. Zhao, Z. Xiang, C. Wang, J. Zhang, B. Yang, *Mater. Lett.* **2007**, *61*, 363. doi:10.1016/J.MATLET.2006.04.064

[27] M. Guo, P. Diao, S. Cai, *J. Solid State Chem.* **2005**, *178*, 1864. doi:10.1016/J.JSSC.2005.03.031

[28] Z.-j. Wang, Y. Xie, C.-j. Liu, *J. Phys. Chem. C* **2008**, *112*, 19818. doi:10.1021/JP805538J

[29] H. Guo, H. Qian, S. Sun, D. Sun, H. Yin, X. Cai, Z. Liu, J. Wu, T. Jiang, X. Liu, *Chem. Cent. J.* **2011**, *5*, 1. doi:10.1186/1752-153X-5-1

[30] M. Najafi, Y. Yousefi, A. A. Rafati, *Separ. Purif. Tech.* **2012**, *85*, 193. doi:10.1016/J.SEPPUR.2011.10.011

[31] M. D. Donohue, G. L. Aranovich, *Adv. Colloid Interface Sci.* **1998**, *76–77*, 137. doi:10.1016/S0001-8686(98)00044-X

[32] P. L. Llewellyn, U. Ciesla, H. Decher, R. Stadler, F. Schuth, K. K. Unger, *Stud. Surf. Sci. Catal.* **1994**, *84*, 2013. doi:10.1016/S0167-2991(08)63762-3

[33] Y. Zhu, J. Shi, H. Chen, W. Shen, X. Dong, *Microporous Mesoporous Mater.* **2005**, *84*, 218. doi:10.1016/J.MICROMESO.2005.05.001

[34] L. L. Lv, W. H. Geng, C. Wang, Z. Y. Xie, Y. J. Zhao, Y. Guan, X. D. Bai, L. G. Sun, *Adv. Mat. Res.* **2013**, *668*, 207.

[35] J. Coates, in *Encyclopedia of Analytical Chemistry* (Ed. R. A. Meyers) **2000**, pp. 10815–10837 (John Wiley & Sons, Ltd: Chichester).

[36] C. P. Sibu, S. R. Kumar, P. Mukundan, K. G. K. Warrier, *Chem. Mater.* **2002**, *14*, 2876. doi:10.1021/CM010966P

[37] R. Georgekutty, M. K. Seery, S. C. Pillai, *J. Phys. Chem. C* **2008**, *112*, 13563. doi:10.1021/JP802729A

[38] H.-L. Xia, F.-Q. Tang, *J. Phys. Chem. B* **2003**, *107*, 9175. doi:10.1021/JP0261511

[39] E. G. Pantohan, R. T. Candidato, R. M. Vequizo, *J. Appl. Sci. Agric.* **2014**, *9*, 389.

[40] A. K. Zak, M. E. Abrishami, W. H. A. Majid, R. Yousefi, S. M. Hosseini, *Ceram. Int.* **2011**, *37*, 393. doi:10.1016/J.CERAMINT.2010.08.017

[41] M. Öztas, *Chin. Phys. Lett.* **2008**, *25*, 4090. doi:10.1088/0256-307X/25/11/069

[42] J. S. Reed, *Introduction to the Principles of Ceramic Processing* **1986** (John Wiley & Sons: New York, NY).

[43] G. A. Parks, *Chem. Rev.* **1965**, *65*, 177. doi:10.1021/CR60234A002

[44] P. S. Bedi, A. Kaur, *World J. Pharm. Pharm. Sci.* **2015**, *4*, 1177.

[45] A. Degen, M. Kosee, *J. Eur. Ceram. Soc.* **2000**, *20*, 667. doi:10.1016/S0955-2219(99)00203-4

[46] P.-S. Keng, S.-L. Lee, S.-T. Ha, Y.-T. Hung, S.-T. Ong, in *Green Materials for Energy, Products and Depollution* (Eds E. Lichtfouse, J. Schwarzbauer, D. Robert) **2013**, pp. 335–414 (Springer: Dordrecht).